Bioactive Scaffolds Mimicking Natural Dentin Structure

A. Vallés Lluch,[1] A. Campillo Fernández,[1] G. Gallego Ferrer,[1,2,3] M. Monleón Pradas[1,2,3]

[1] Center for Biomaterials and Tissue Engineering, Universidad Politécnica de Valencia, 46022 Valencia, Spain

[2] Regenerative Medicine Unit, Centro de Investigación Príncipe Felipe, 46013 Valencia, Spain

[3] Networking Research Center on Bioengineering, Biomaterials and Nanomedicine, Valencia, Spain

Received 30 April 2008; revised 30 September 2008; accepted 3 October 2008
Published online 15 December 2008 in Wiley InterScience (www.interscience.wiley.com). DOI: 10.1002/jbm.b.31272

Abstract: Organic scaffolds of poly(ethyl methacrylate-*co*-hydroxyethyl acrylate) [P(EMA-*co*-HEA)] 70/30 wt % ratio, with varying proportions of silica SiO_2 from 0 to 20 wt % and aligned tubular pores, were prepared using a fiber-templating fabrication method, with the aim of mimicking structure and properties of the mineralized tissue of natural dentin. Precursors of the copolymer and silica were simultaneously polymerized in a sol–gel process within the fiber template, which was eventually eliminated to generate homogeneously distributed parallel micrometer-sized pores in the material. Scaffolds of PEMA and PHEA were obtained by the same approach. The scaffolds were characterized by scanning electron microscopy (SEM), Fourier transform infrared spectroscopy, and thermogravimetric analysis. The specific volume was determined by Archimedes' method and the porosity calculated from the geometry. The mechanical properties were analyzed in tensile and compressive modes. The bioactivity of the scaffolds with 15 wt % SiO_2 was tested by immersion in simulated body fluid (SBF) for 7 days followed by immersion in 2× SBF for 7 days. These scaffolds were afterwards characterized by SEM, energy dispersive spectroscopy, and compression assays. Percentages of silica above 10 wt % reinforced mechanically the copolymer, evidenced by the hindrance of the long range motions of the organic chains, altered shrinkage and swelling, and meanwhile conferred bioactivity to its surface. These tubular porous structures, which resemble natural dentin with regard to its structure and properties and induce the precipitation of apatite on their surfaces *in vitro*, are expected to facilitate the integration in the host mineralized tissue, to stimulate cell growth and to be useful as guiding scaffolds for *in vivo* dentin regeneration.
 J Biomed Mater Res Part B: Appl Biomater 90B: 182–194, 2009

Keywords: scaffold; dentin; nanocomposite; bioactivity; simulated body fluid (SBF); hydroxyapatite

INTRODUCTION

Dentin is the mineralized tissue below enamel that constitutes the body of teeth. It is composed of approximately 30 vol % of an organic matrix, consisting mostly of type I collagen, 50 vol % of an inorganic reinforcing phase of carbonated apatite, and 20 vol % of a fluid similar to plasma.[1] The pulp, a loose connective tissue that provides dentinogenic, nutritive, sensory, and defensive functions to the tooth, supports it. Dentin is deposited by odontoblasts, a kind of cylindrical cells that reside in the pulp, forming an epithelial layer in its periphery just below dentin. One of the morphological features of dentin is the presence of small parallel tubules of few microns, which traverse it from the pulp chamber to the region just below the dentin–enamel junction. Dentinal tubule diameters are ~2.5 μm near the pulp and 0.9 μm near the dentin–enamel junction. Each tubule contains the apical prolongation of one odontoblast.[2,3]

When an oral disease such as caries is deep and the pulp is exposed, either direct pulp capping with calcium hydroxide or root canal therapy are performed, which imply the replacement of the affected dental tissue by synthetic materials.[3,4] Few of these materials share the same physical or chemical characteristics of the natural replaced tissue, and these cavity restorations tend to fail mechanically. Microleakage of the composite/tooth interface with the penetration of bacterial enzymes, bacteria, fluids, and ions tend to produce hypersensitivity and a secondary caries.[2,4]

Correspondence to: A. Vallés Lluch (e-mail: avalles@ter.upv.es)
Contract grant sponsor: Consellería de Empresa, Universidad y Ciencia, Valencia; contract grant number: AE/07/050

Alternative therapies based on tooth tissue engineering have recently been proposed; they demonstrate that certain synthetic scaffolds can induce the regeneration of dentin/pulp tissue.[3–8] Young et al. and Yelick and Vacanti seeded different scaffolds of polylactic and polyglycolic acids with porcine pulp cells and implanted them in the omentum of athymic rats.[5,6] Their histological analyses revealed the regeneration of the two major mineralized structures of the tooth: dentin and enamel. Another study demonstrated that polyglycolic acid scaffolds are more efficient than collagen or alginate scaffolds when cultured *in vitro* with seeded human dental pulp fibroblasts (HPF).[3] These HPF survived when implanted into subcutaneous sites in immunocompromised mice and synthesized type I collagen, cellular fibronectin, and expressed genes implicated in transducing bone morphogenetic protein signals.[7] Some regenerative therapies are based on the stimuli for the differentiation of pulpal progenitor cells to odontoblasts. In Ref. 8, it has been demonstrated that the transforming growth factor TGF-β1 delivered from alginate scaffolds was capable of inducing new odontoblast-like cell differentiation from pulpal progenitor cells.

None of these strategies presents a structure of the scaffold that intends to reproduce that of natural dentin. On the contrary, this work presents a new synthetic nanocomposite scaffold that mimics the tubular porous morphology of natural dentin and has a potential bioactivity. These features aim at the invasion by new odontoblast prolongations of the pores of the scaffold when implanted *in vivo*, which would be able to fabricate new natural dentin while providing a very good adhesion between the scaffold and the surrounding natural tissue. The bioactive or bone-bonding materials form a layer of hydroxyapatite (HAp) on their surface when implanted in the body, through which they bond to the living bone. The characterization of the properties of these new scaffolds is presented herein.

On the basis of the fiber-templating fabrication method,[9,10] we synthesized different scaffolds with tubular aligned pores of diameters about 8 μm. The scaffolds were made of a hybrid organic–inorganic nanocomposite, with an inorganic silica (SiO_2) phase included in an organic matrix, both phases polymerized simultaneously in a sol–gel process.[11] The sol–gel reaction is a polymerization process in which a silica precursor, tetraethoxysilane (TEOS), hydrolyses and condenses to form a network. Under acid-catalyzed reaction conditions and with a stoichiometrically deficient amount of water, it is known that the condensation rate is much greater than the production of silanols by the hydrolysis reaction, and the silica forms an extremely fine network in the nanometer scale.[12] As organic component, a hydrophobic/hydrophilic copolymer of ethyl methacrylate (EMA) and hydroxyethyl acrylate [P(EMA-*co*-HEA)] was chosen according to two requirements: good mechanical properties provided by the EMA component and hydrophilicity of the hydroxyethyl acrylate (HEA) comonomers needed for a good miscibility of the TEOS mixture[13] and for cell interaction. The resulting hybrids were optically transparent with high mechanical properties because of the SiO_2 network and its ability to transport oxygen and nutrients through the water absorbed in them.

Since the discovery of 45S5 Bioglass® (24.5 wt % Na_2O–24.5 wt % CaO–45 wt % SiO_2–6 wt % P_2O_5) by Hench in 1971,[14] most of the studies with bioactive glasses and glass ceramics were devoted to the understanding of the mechanism of apatite formation and the roles of the glass constituents, and to obtain simpler bioactive compositions based on the initial system $Na_2O—CaO—SiO_2—P_2O_5$.[15–22] It was found that silica dissolution and silanol groups (Si—OH) formation are the key factors to induce the apatite nucleation and layer deposition on the surface of these materials,[23,24] even with Ca and P absent from the composition. The use of bioactive glasses as implant materials or in manufacturing medical devices was, though, limited by their poor mechanical properties. These finding brought the idea that organic modification of silicates would enable development of new materials with applications in the field of mineralized tissue regeneration, showing bioactivity and compatible mechanical properties. Different approaches have been explored through the preparation of organic/inorganic hybrids, in which the inorganic phase is incorporated into an organic polymeric matrix; for example, hybrid systems that employ as inorganic phase bioactive glasses,[25,26] HAp[27–29] or pure silica[25] in the form of particles or fibers. In the last years, some studies have been devoted to the study of hybrid nanocomposites, with the aim of combining the properties of both phases at the nanoscale level. Polymer/silica nanocomposites have been prepared by physically mixing silica nanoparticles with polymers,[30,31] by copolymerization of an organic monomer in the presence of organically functionalized preformed silica nanoparticles,[11,32] or as organically modified silicates obtained through sol–gel processing, employing alkoxysilanes as starting materials in combination with a silica precursor[33] or an organic monomer[34,35] to promote chemical bondings. Their potential bioactivity has been reported. In line with these studies, the bioactivity of the scaffolds here presented could be a crucial parameter for the good integration of the scaffolds in the host dentin tissue (preventing recurring caries, breakdown, and infiltration) and for providing stimuli for differentiation of the pulpal surrounding cells when implanted *in vivo*.

MATERIALS AND METHODS

Materials

The hybrid materials were obtained by copolymerization of ethyl methacrylate (EMA; 99%, Aldrich) and hydroxyethyl acrylate (HEA; 96%, Aldrich), with 70/30 wt % of monomers ratio, during the simultaneous acid-catalyzed sol–gel polymerization of TEOS (98%, Aldrich), following a similar procedure to that described, for example, by Hajji et al.

TABLE I. Sample Composition and Properties of the Matrices: Residue at 700°C ($w_{700°C}$), Equilibrium Water Content With Respect to the Mass of Dry Sample (EWC) and to the PHEA Content (EWC′), and Temperature of the tan δ Maximum (T_α)

Composition	Sample	$w_{700°C}$ (%)	EWC (%)	EWC′ (%)	T_α (°C)
P(EMA)	PEMA	0.36	1.18	–	101.37
P(HEA)	PHEA	0.92	202.52	202.52	–
P(EMA-*co*-HEA) 70/30 wt %	H00	0.52	8.34	27.80	67.20
P(EMA-*co*-HEA) 70/30 wt %/5% SiO_2	H05	4.99	8.11	28.44	71.35
P(EMA-*co*-HEA) 70/30 wt %/10% SiO_2	H10	10.64	7.66	28.36	77.67
P(EMA-*co*-HEA) 70/30 wt %/15% SiO_2	H15	14.61	6.92	27.13	77.48
P(EMA-*co*-HEA) 70/30 wt %/20% SiO_2	H20	19.56	6.74	28.07	84.57

for another polymer.[11] First, both organic monomers were mixed together with a 0.5% monomer weight of ethylene glycol dimethacrylate (98%, Aldrich) as crosslinking agent and a 2% monomer weight of benzoyl peroxide (97%, Fluka) as thermal initiator. Separately, a solution was prepared by mixing TEOS with distilled water and hydrochloric acid (37%, Aldrich) in the molar ratio of 1:2:0.0185, respectively. At low pH, hydrolysis reactions are favored over condensations, thus leading to a fine weakly branched or crosslinked silica structure.[11] After 30 min of stirring, both solutions were mixed and stirred for additional 30 min. The silica content was changed from 0 to 5, 10, 15, and 20 wt % by controlling the (EMA+HEA)/TEOS ratio and assuming that the sol–gel reactions were complete.

Glass tubes of 3-mm inner diameter were cut in 3.5-cm long pieces, stuffed with 10-μm diameter polyacrylonitrile (PAN, Montefibre), aligned fibers and sealed on one side. The previously obtained mixtures were vacuum-injected in these glass molds, which were immediately capped and placed in an oven for polymerization at 60°C for 21 h followed by postpolymerization at 90°C for 18 h. Afterwards, the PAN fibers were eliminated from the materials by dissolution in *N*,*N*-dimethylformamide (99.8%, Aldrich). The resulting scaffolds were washed in ethanol to remove residuals and unreacted monomers and finally dried in a vacuum desiccator at 80°C until constant weight.

Thus, the scaffolds of poly(ethyl methacrylate-*co*-hydroxyethyl acrylate) [P(EMA-*co*-HEA)] 70/30 wt % with varying proportions of silica (SiO_2), up to 20 wt %, with aligned tubular pores were obtained. Scaffolds of poly(ethyl methacrylate) (PEMA) and poly(hydroxyethyl acrylate) (PHEA) were also obtained by the same procedure. The composition of the different samples is given in Table I. Hereafter, the hybrids will be referred to as H*x*, with *x* being the weight percentage of silica.

In order to determine the properties of the nanocomposite matrix of the scaffolds, bulk sheets of 0.8 mm thickness of the different compositions were synthesized by the same procedure. The mold consisted in two glass plates with a rubber wire in between. Once polymerized, the samples were rinsed in boiling ethanol/water 50/50 vol % mixture for 24 h and dried. All the obtained materials were optically transparent and increasingly rigid with the silica content.

Methods

Morphological analysis of the scaffolds was undertaken by scanning electron microscopy (SEM), in a JSM-6300 microscope, with the samples previously sputter-coated with gold, 15 kV of acceleration voltage and 15 mm of working distance. SEM images were obtained before and after eliminating the PAN fibers, in longitudinal and transversal sections.

Fourier transform infrared (FTIR) spectra of the bulk samples were collected in the attenuated total reflection mode between 650 and 4000 cm^{-1} with a Thermo Nicolet Nexus spectrometer, operating with a 4 cm^{-1} resolution and averaging 128 scans, to analyze structural characteristics.

Thermogravimetric analyses (TGA) of the bulk samples were carried out in a TA-SDT Q600 thermobalance, at 10°C/min from 25 to 1000°C in a nitrogen atmosphere, to determine the actual inorganic contents and determine the thermodecomposition profiles. Samples of ~7 mg were analyzed each time.

A small piece of the 15 wt % SiO_2 hybrid scaffold was pyrolized in a tubular oven (Gallur, Spain), programmed with a 3 h ramp to 1000°C followed by a 4-h isotherm, under oxygen atmosphere. SEM images of the residue were obtained and compared with those of the original scaffold.

A Mettler AE 240 balance with a sensitivity of 0.01 mg with a Mettler ME 33360 accessory kit was used to measure the specific volume of the bulk samples through Archimedes' principle (the apparent weight of a solid immersed in a liquid decreases by an amount equal to the weight of the liquid that it displaces). The dry samples were weighed in air and immersed in *n*-octane (95%, Fluka, $\rho_{n\text{-octane}} = 0.702$ g/cm^3) at room temperature. The specific volume of each composition was determined in triplicate as the volume of *n*-octane displaced divided by the mass of the sample in air:

$$v = \frac{V_{\text{displaced}}}{m_{\text{in air}}} = \frac{(m_{\text{in air}} - m_{\text{in } n-\text{octane}})/\rho_{\eta-\text{octane}}}{m_{\text{in air}}}$$

The porosity of the scaffolds was calculated afterwards through the specific volume of the respective bulk sample, weight, and total volume (calculated through the measurement of the height and diameter) of the scaffolds, in duplicate.

The swelling of the bulk samples in water was quantified by weighing the samples dried and after equilibration to constant weight immersed in distilled water at room temperature using the previously mentioned balance. The equilibrium water content (EWC) was defined as the ratio between the mass of water in the sample and the mass of the dry sample.

Dynamic mechanical spectroscopy (DMS) analysis was performed on bulk samples in a Seiko DMS210 instrument. Measurements were carried out in the tensile mode at 1°C/min from 25 to 200°C at a frequency of 1 Hz. Samples were rectangular, $\sim 25 \times 6.5 \times 0.8$ mm^3.

Mechanical compression assays were performed on the scaffolds in the longitudinal direction (the tubular pores in the vertical direction, which will be their position when the scaffold is implanted in the tooth) in a Seiko TMA/SS6000 equipment, from 0.05 to 150 g, at 10 g/min, at room temperature. Measurements were repeated five times for each composition. Samples were cylindrical, 3 mm in diameter (2.6 mm in the case of PHEA) and ~3 mm in height.

The ability of the H15 hybrid scaffold to form apatite on its surface was tested *in vitro*, at 37°C in a simulated body fluid (SBF) solution, with ion concentrations nearly equal to those of the human blood plasma, by the method proposed by Kokubo and coworkers.[23,36] The bioactivity of the different samples of the series (as bulk sheets) was assessed by immersion in SBF in a previous work, (unpublished observation) and the results were correlated with the different silica nanostructures and consequently with the composition. In order to obtain the SBF, two solutions were prepared. Solution 1 consisted of 1.599 g of NaCl (99%, Scharlau), 0.045 g of KCl (99%, Scharlau), 0.110 g of $CaCl_2 \cdot 6H_2O$ (99%, Fluka), and 0.061 g of $MgCl_2 \cdot 6H_2O$ (Fluka) in deionized ultrapure water (Scharlau) up to 100 mL. Solution 2 was prepared by dissolving 0.032 g of $Na_2SO_4 \cdot 10H_2O$ (Fluka), 0.071 g of $NaHCO_3$ (Fluka), and 0.046 g of $K_2HPO_4 \cdot 3H_2O$ (99%, Aldrich) in water up to 100 mL. Both solutions were buffered at pH 7.4, by adding the necessary amounts of aqueous 1*M* tris-hydroxymethyl aminomethane [$(CH_2OH)_3CNH_2$; Aldrich] and 1*M* hydrochloric acid (HCl; 37%, Aldrich). Then, both solutions were mixed to obtain SBF with the corresponding molar ion concentrations: 142 m*M* Na^+, 5.0 m*M* K^+, 1.5 m*M* Mg^{2+}, 2.5 m*M* Ca^{2+}, 148.8 m*M* Cl^-, 4.2 m*M* HCO_3^-, 1.0 m*M* HPO_4^{2-}, 0.5 m*M* SO_4^{2-}. Pieces of scaffolds of 3 mm length were suspended from a cotton thread inside closed glass vials filled with SBF. The ratio of geometric surface area of scaffold (without considering the inner pores surface) to solution volume was 0.12 mL/mm^2. The SBF solution was not renewed during the first 7 days. Afterwards, the ion concentrations were adjusted to twice those of SBF (2×SBF) by dissolving the same previous quantities of salts in half the volume of deionized ultrapure water. The solution was renewed 2–3 days each, in order to provide more favorable conditions for apatite deposition.[37,38] The body fluid is already supersaturated with respect to the apatite under normal condition. Once the apatite nuclei are formed, they can grow spontaneously by consuming the calcium and phosphate ions from the surrounding body fluid. The 2×SBF solution, having ion concentrations twice as large as those of SBF, increases the degree of supersaturation to apatite while maintaining the Ca/P atomic ratio. In such a solution, apatite is expected to grow more rapidly. It is a usual procedure to incubate the materials in SBF in a first treatment to form HAp nuclei (nucleation process), and afterwards soak them in modified SBFs with ion concentrations 1.5 or 2 times those of the SBF (1.5×SBF and 2×SBF, respectively), with periodical renovation, to make the apatite nuclei grow more rapidly (growth stage).[37–39]

Samples were withdrawn from the SBF after 7 and 14 days, rinsed with water, room-conditioned, and finally dried in a vacuum desiccator at 80°C. SEM micrographs of the apatite-covered scaffolds were taken on the transversal surface and on the longitudinal fractured surface. Energy dispersive spectroscopy (EDS) was carried out in the same microscope, with the samples previously sputter-coated with carbon, 10 kV of acceleration voltage, and 15 mm of working distance. Silicon was employed as an optimization standard. Mechanical compression assays were performed on the H15 scaffolds after 14 days in SBF, following the method described earlier.

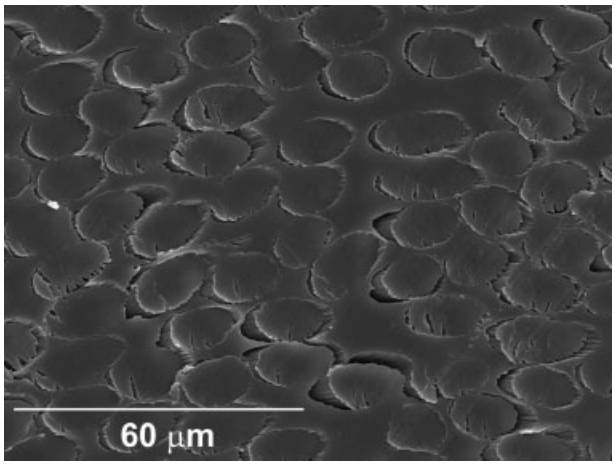

Figure 1. SEM image of a H15 scaffold before eliminating the fiber template.

RESULTS

Scanning Electron Microscopy

Figure 1 shows a SEM image of the H15 scaffold before eliminating the fiber template. Figure 2 displays the micrographies of some scaffolds after fiber dissolution. The transversal sections show in all cases a homogeneous distribution of cylindrical pores of ~8 μm of diameter, except in the case of PHEA, where the majority of the pores collapse and the diameter of the remaining pores decreases due to the shrinkage of the scaffold.

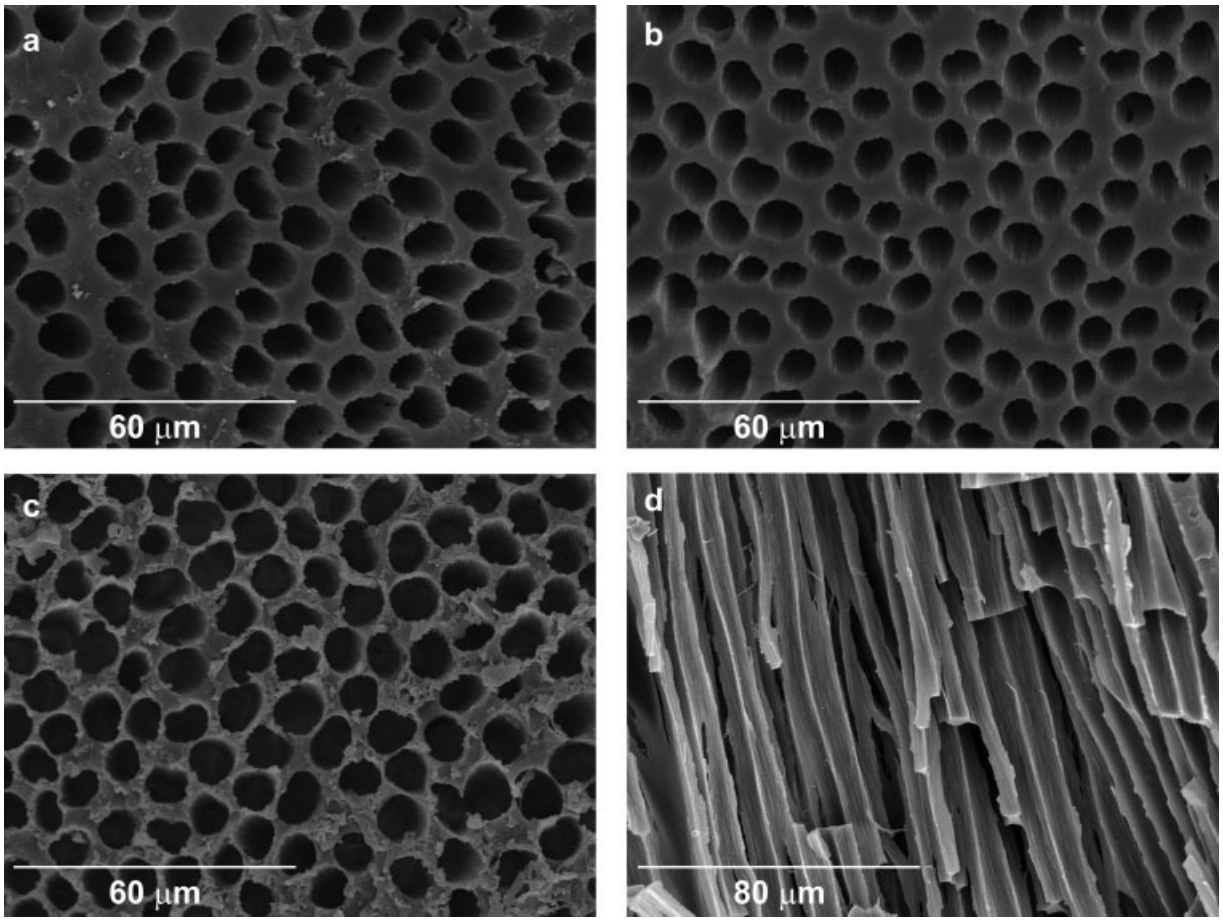

Figure 2. SEM images of scaffolds of (a) PEMA, (b) H00, (c,d) H15 in transversal and longitudinal section, respectively.

Fourier Transform Infrared Analysis

Figure 3 displays the FTIR spectra of PEMA and PHEA polymers and the P(EMA-*co*-HEA) copolymer. The spectrum of PHEA shows a broad band between 3100 and 3700 cm^{-1}, characteristic of the OH groups. This band does not appear in the copolymer spectrum. The strong peak at 1700 cm^{-1} appearing in all cases corresponds to the C=O bond. Between 1500 and 650 cm^{-1}, the spectra of the polymers are quite complex.

Figure 4 shows the FTIR spectra of the different nanocomposites. The intensity of the peaks at 1100 cm^{-1} and 800 cm^{-1} (Si—O—Si asymmetric and symmetric stretching, respectively) and 950 cm^{-1} (Si—OH stretching) increases proportional to the silica content. These peaks are well defined and characterize the silica phase.[11,31,40–44] Si—O—C bond peaks due to heterocondensation reactions at organic–inorganic interfaces could also be present, but they cannot be confirmed from FTIR assays owing to the

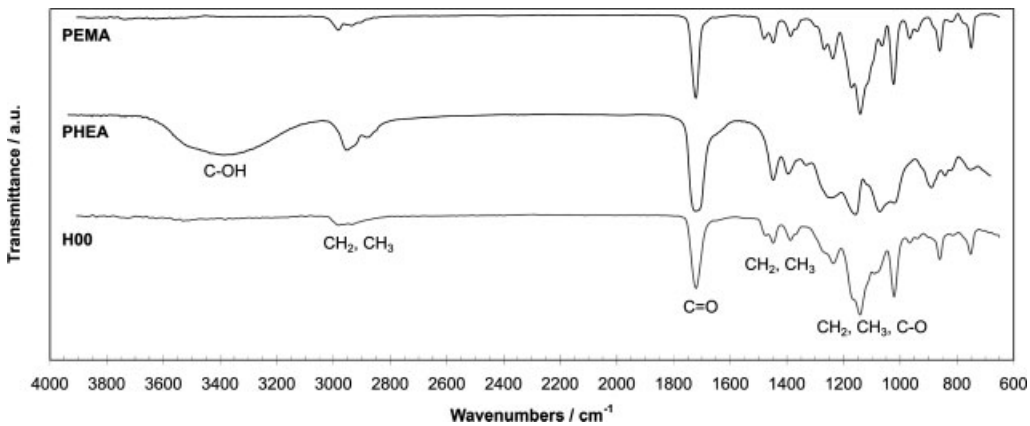

Figure 3. FTIR spectra of PEMA, PHEA, and H00 in the 650–4000 cm^{-1} region.

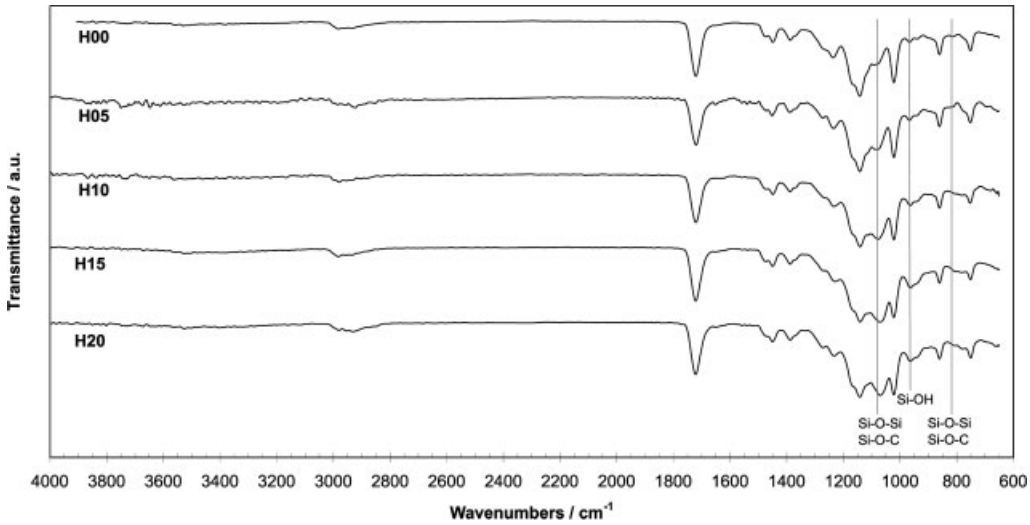

Figure 4. FTIR spectra of the hybrid nanocomposites, with silica contents ranging from 0 to 20 wt %.

complexity of the spectra in this region. Hajji et al.[11] could not find evidence of interfacial covalent Si—O—C bonds in PHEMA/SiO_2 nanohybrids, neither by FTIR nor by NMR, and concluded that no extensive hybrid bonding had taken place.

Thermogravimetry

Figure 5(a) shows the mass loss as a function of temperature for both homopolymers and the copolymer. Decompositions of both PEMA and PHEA polymers seem to take place in several stages. PEMA decomposes between 210 and 395°C, whereas PHEA decomposes at higher temperatures and, more gradually, in the 340–550°C interval. The curve of the copolymer lies in the 220–550°C temperature interval, between those corresponding to both polymers. At 550°C, all of them have totally decomposed without leaving residues.

The thermogravimetric plots of the silica nanocomposites are displayed in Figure 5(b). The weight loss also occurs in all cases in several steps. A shift of the curves to lower temperatures can be observed as the silica content increases.

The overall weight loss decreases with the nominal silica content. The experimental percentages of residues have been determined at 700°C ($w_{700°C}$) for the different samples and are listed in Table I. They agree well with the nominal inorganic contents in the hybrids in all cases.

Pyrolysis

This technique has been employed elsewhere[45] to analyze the oxide network connectivity of silica gels. Figure 6 shows the SEM images of the residue of pyrolysis of the H15 scaffold with the purpose of comparing it with the

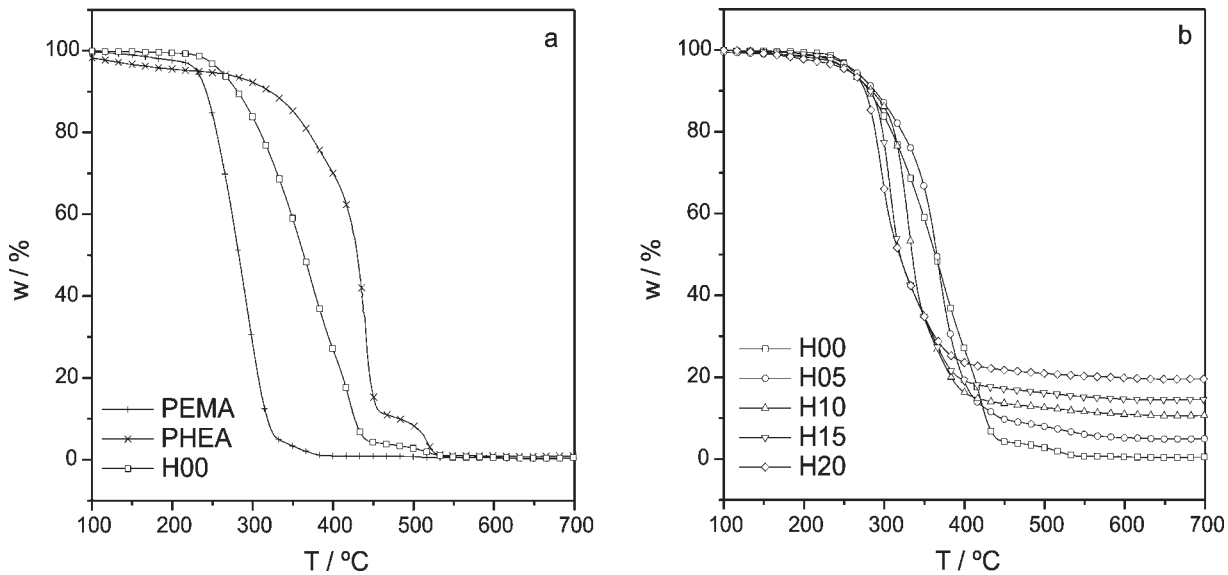

Figure 5. Mass loss (w) as a function of temperature for (a) (+) PEMA, (×) PHEA, and (□) H00; (b) (□) H00, (○) H05, (△) H10, (▽) H15, and (◇) H20 hybrids.

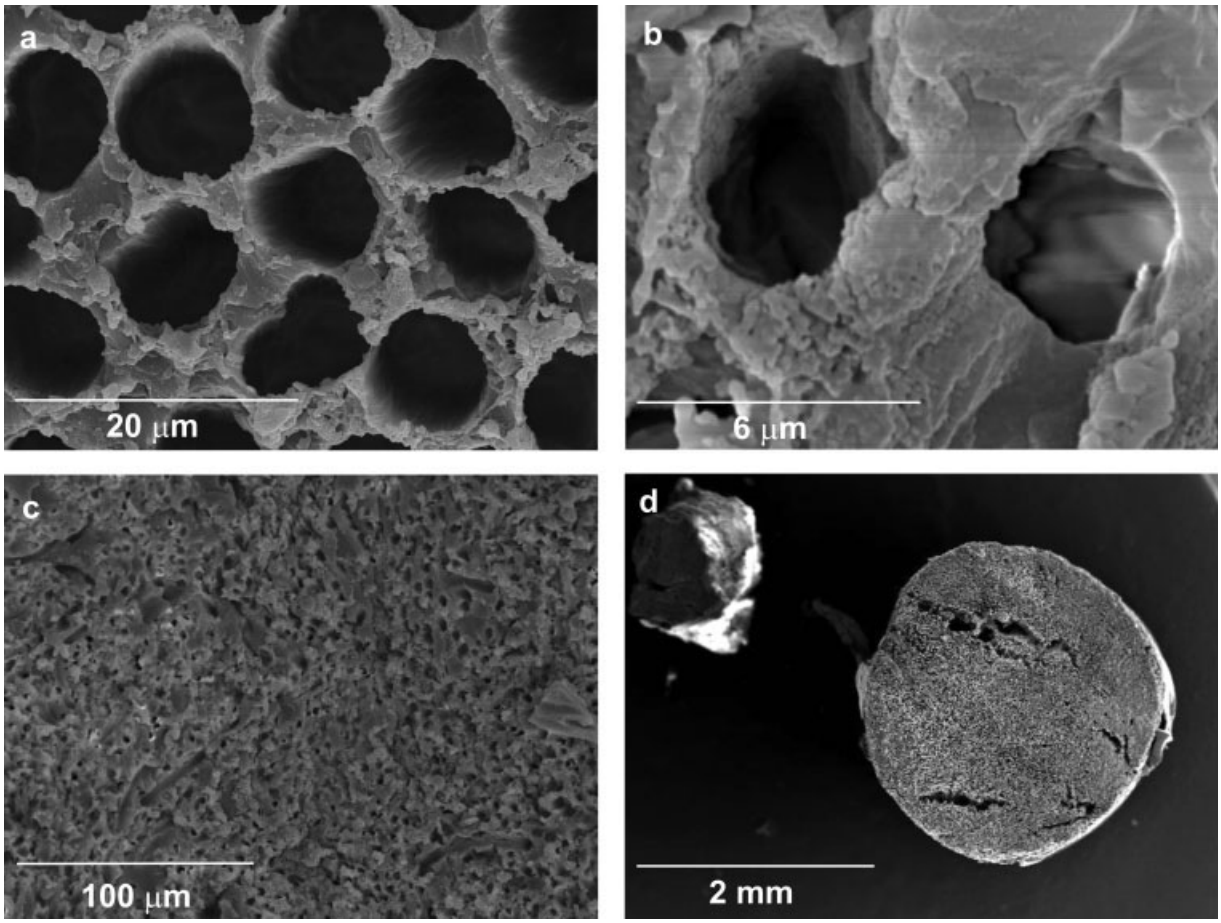

Figure 6. SEM micrographies of (a) H15, (b,c) H15 pyrolyzed at 1000°C, (d) H15 pyrolyzed, next to the original scaffold on the right.

original scaffold. The residue is a scaffold and maintains the original shape but shrinks, that is, the silica network contracts as the organic phase pyrolyzes. The original scaffold of parallel channels [Figure 6(a)] collapses somewhat [Figure 6(b)], leaving a structure of smaller diameter pores (~4 μm).

Specific Volume

The dependence of the specific volume of the nanocomposites on the silica content, v, is shown in Figure 7. The obtained values for PEMA and PHEA polymers are 0.89 and 0.77 cm^3/g, respectively. The specific volume decreases linearly with the silica content from 0.85 for H00 to 0.79 cm^3/g for H20. Error bars representing the standard deviation are included, as are the size of the symbols used in the plot.

Porosity

The porosity, π, has been calculated for each scaffold according to the following equation

$$\pi = \frac{V_{\text{pores}}}{V} = \left(1 - \frac{m_{\text{scaff}} v}{V}\right) \times 100$$

where V_{pores} is the pore volume, V is the overall sample volume, v is the specific volume of the corresponding bulk sample (previously calculated), and m_{scaff} is the mass of the scaffold. The porosities obtained for the homopolymer scaffolds were 49.8% for PEMA and 14.5% for PHEA, and for the copolymer the porosity lies between them (Table II). The porosity of the hybrids increases in comparison with the copolymer, taking values in the vicinity of 50%, and is scarcely influenced by the different silica content, increasing slightly with it (Table II).

Water Sorption by Immersion

Table I displays the EWC of the bulk hybrids referred to the dry mass of the sample (EWC) and referred to the HEA mass in the sample (EWC′) defined as

$$\text{EWC}' = \frac{m_{\text{water}}}{m_{\text{HEA}}} = \frac{m_{\text{water}}/m_{\text{dry}}}{m_{\text{HEA}}/m_{\text{dry}}} = \frac{\text{EWC}}{x_{\text{HEA}}}$$

where x_{HEA} is the mass fraction of HEA in the sample. The EWCs for the PEMA, PHEA, and H00 polymers are 1.18%, 202.52%, and 8.34%, respectively, and slightly decreases with the silica content. The EWC′ values do not seem to differ significantly with the amount of silica.

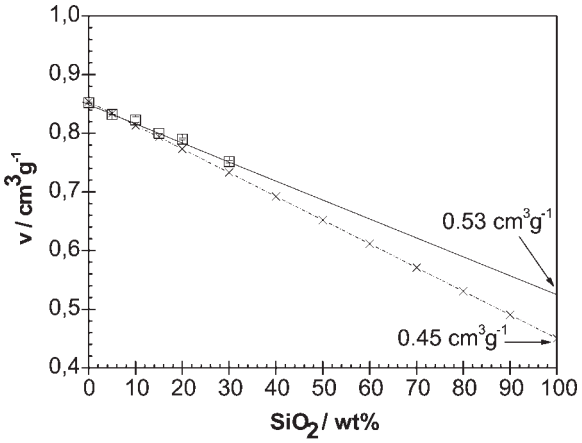

Figure 7. (□) Specific volume (v) of the hybrids as a function of the silica percentage, (—) linear regression and extrapolation for a sol–gel pure SiO_2, (×) specific volume predicted from the v values of PEMA, PHEA, and pure SiO_2 glass obtained by curing at 900°C (the last one taken from Ref. 12).

Dynamic Mechanical Analysis

Figure 8 shows the dynamic mechanical spectra obtained for both bulk homopolymers and for the copolymer, at 1 Hz of frequency and in the temperature range of 25–200°C, in terms of the storage modulus (E') and loss tangent (tan δ).

The curves corresponding to the copolymer lie between the ones corresponding to both homopolymers. The glass–rubber relaxation of the copolymer appears as a sharp single drop of the storage modulus, from 40 to 80°C, to very low values, with the corresponding maximum of the loss tangent at ~67°C.

The spectra corresponding to the nanocomposites are displayed in Figure 9. The glass–rubber relaxation progressively broadens and shifts to higher temperatures when the silica content increases. At the same time, the maximum in tan δ and the area under its peak decrease. Besides, the rubbery plateau modulus is increasingly higher, mainly from 10 wt % of silica content onwards. The values of the storage modulus of the samples at 150°C ($E'_{150°C}$) have been plotted in the inset of Figure 9 as a function of silica content. The temperatures of the maxima of tan δ (T_α) have been listed in Table I.

TABLE II. Properties of the Scaffolds: Porosity (π) and Elastic Modulus (E)

Sample	π (%)	E (MPa)
PEMA	49.76	3788
PHEA	14.55	161
H00	37.26	3685
H05	47.93	3342
H10	50.96	5380
H15	52.25	6156
H20	53.71	6238

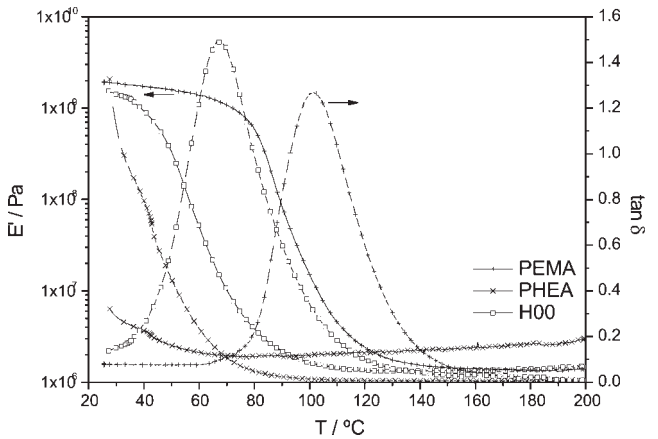

Figure 8. (—) Temperature dependence of the storage modulus (E') and (– – –) loss tangent (tan δ) of (+) PEMA, (×) PHEA, and (□) H00 samples.

Coating of Bone-Like Apatite

Figures 10 and 11 show the SEM images of the H15 hybrid scaffolds, after 7 and 14 days of immersion in SBF, respectively. After 7 days in SBF, some scattered deposits are visible in the transversal section, but nothing in the interior surfaces of the pores. After 14 days, the exterior transversal surface is covered with needle-shaped HAp polycrystals, forming cauliflower structures typical of bioactive glasses[23,41,46–48] and similar to those deposited on bulk samples of the same composition (unpublished observation) with an average diameter of 1 μm, which do not clog up the pores cavities. Scattered agglomerates of cauliflowers (with greater diameter) of what seem to be subsequent layers are superposed on the first homogeneous coating. The longitudinal fracture shows that the surface of the tubular pores is almost completely coated with the first continuous apatite layer after 14 days in SBF. It was not possible to quantify the amount of HAp gravimetrically because of the small increase in weight of the samples after the apatite deposition. An average Ca/P ratio of 1.56 was obtained by EDS (spectra

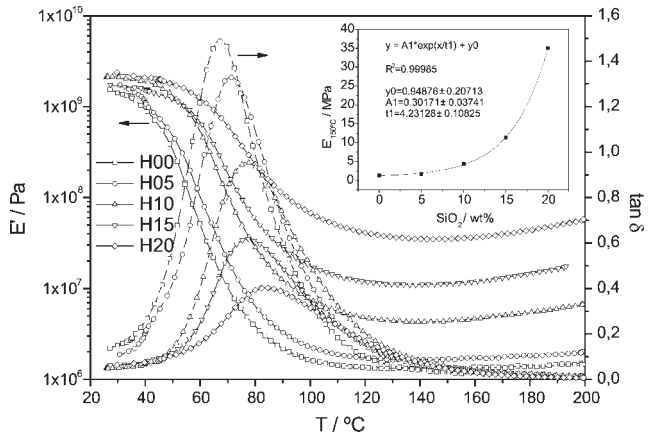

Figure 9. (—) Temperature dependence of the storage modulus (E') and (– – –) loss tangent (tan δ) of (□) H00, (○) H05, (△) H10, (▽) H15, and (◇) H20. Inset: dependence of the storage modulus of the samples at 150°C ($E'_{150°C}$) with the silica content.

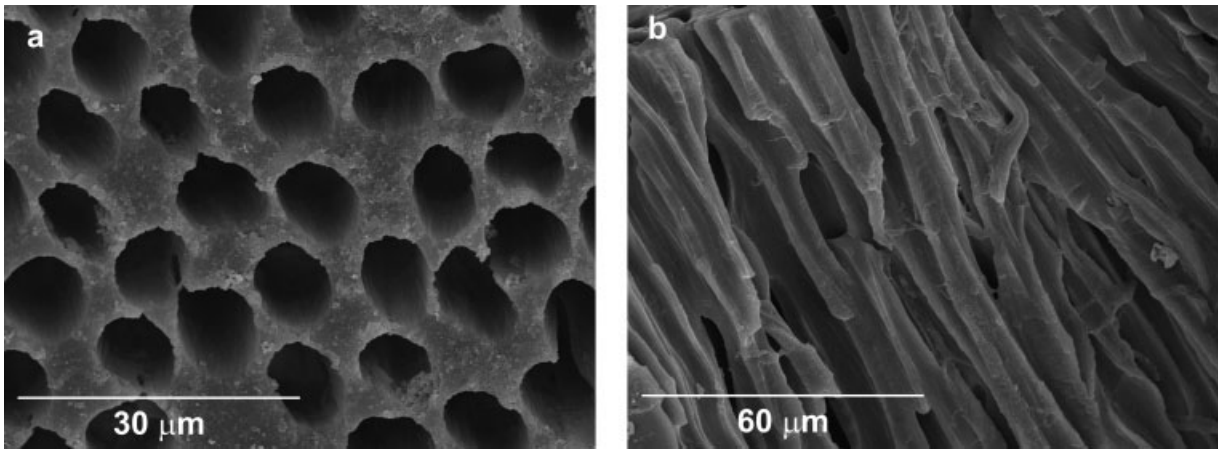

Figure 10. SEM images of the H15 scaffold after 7 days in SBF. (a) Transversal section and (b) longitudinal fracture.

not shown), which is slightly lower than the Ca/P ratio of stoichiometric HAp,[23] 1.67. Other elements from the SBF like Na and Cl were also detected.

Compression Tests

The elastic moduli of the scaffolds (E) have been obtained from the initial slope of the stress–strain curves, and have been listed in Table II. The values obtained for the homopolymers are 3788 MPa for PEMA and 161 MPa for PHEA. The elastic modulus of the H00 scaffold is very similar to that of PEMA, slightly decreases for the H05 scaffold, and then increases with the amount of silica up to 6238 MPa for the H20 hybrid sample. The elastic modulus of the H15 scaffold after 14 days in SBF was 8192 MPa, 1.33-fold that of the original H15 scaffold.

DISCUSSION

Hybrid scaffolds of P(EMA-*co*-HEA) 70/30 wt % silica were successfully obtained with varying proportions of silica up to 20 wt %, by the sol–gel method, using a PAN–fiber template that was finally eliminated to leave homogeneously distributed aligned tubular pores of ~8 μm of diameter. The microscope images of the obtained synthetic scaffolds show that they resemble very much natural dentin (see SEM image of natural dentin in Ref. 2, p 1055) with regard to the structure and distribution of the pores, though with a slightly larger pore diameter. In the last years, different alternative tooth therapies have been proposed to induce the regeneration of dentin/pulp tissues. Nevertheless, up to our knowledge, this is the first time a synthetic scaffold that attempts to mimic natural dentin structure is proposed.

It has been reported that the structure of silica in the nanohybrids is bimodal: a family of small pores in the few-nanometer range (around 3 nm) within the elementary silica particles (nanodomains) produced by the liquids acting as a template during the sol–gel reaction[12,49] and another family of pores consisting in the larger spaces (tens of nanometers) left between the aggregates of those smaller elementary particles.[11,45] Therefore, the nanohybrids consist of two phases, the organic polymer phase and the silica

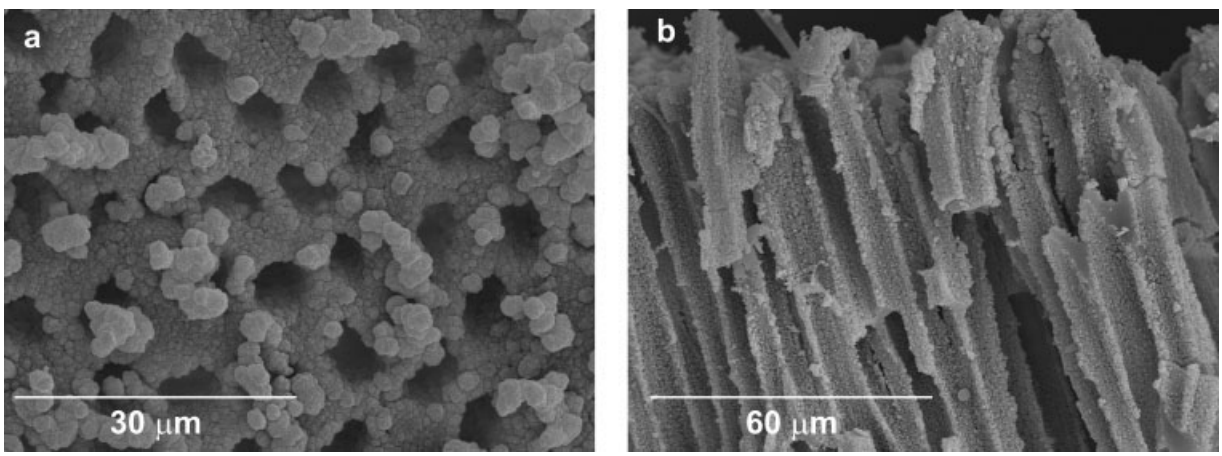

Figure 11. SEM images of the H15 scaffold after 14 days in SBF. (a) Transversal section and (b) longitudinal fracture.

phase in the form of finely interspersed nanoparticles as an interpenetrated network with the organic network. The silica aggregates are uniformly dispersed in the hybrids with low silica contents, and above a certain silica content threshold, these aggregates develop to produce cocontinuous interpenetrated structures where individual silica aggregates are no longer seen. The pores left by the silica phase are occupied by the copolymer network.

The infrared spectra of the P(EMA-*co*-HEA) copolymer and the nanocomposites display the strong peak corresponding to the carboxyl bond (1700 cm^{-1}), but not the broad band characteristic of the hydroxyl groups, which only appears after immersion of the samples in water. This is probably due to a poor contact of the dry samples with the apparatus window, since the rigidity of these samples is higher when dry. At low wavelengths, the peaks characterizing the Si—O—Si and Si—OH bonds of the silica phase overlap with the complex spectra of the copolymer in this region. In any case, the increasing intensity of these silica peaks with the silica content confirms the presence of silica at the surfaces of the hybrids. This is of great significance since silica is expected to confer the bioactivity to the materials,[20] acting as nucleating promotors of HAp crystals when the material will be surrounded by body fluids.

The good agreement of the increasing percentages of TGA residues after complete degradation of the organic polymer with the nominal inorganic contents implies that TEOS efficiently hydrolyzed and condensed to silica during the sol–gel reaction in all cases.

The weight loss of the hybrids during thermal decomposition must be accounted by both the copolymer degradation and the loss of silica bonded groups such as —OH or remaining nonhydrolyzed —OCH_2CH_3, and it occurs in several stages. The thermogravimetric curve of the copolymer lies between those of the homopolymers, and gradually shifts to lower temperatures when increasing the silica content. This decrease in thermal stability of the hybrids when compared to the organic matrix suggests that high temperatures during the measurements allow condensations between noncondensed silanol groups to start again. Water produced in these condensations could be involved in the accelerated scissions of lateral chains in the organic copolymer during the thermogravimetric assays. Costa and Vasconcelos[42] observed a similar behavior in PHEMA/silica composites, and explained it on the basis of a decrease in hydrogen bonding among copolymer chains promoted by the presence of silica. However, other authors[30,44] observed the opposite effect in similar composites and attributed it to a good homogeneity because of nanoscale mixing and to relatively strong inter- and intramolecular hydrogen bonds tethering the silica and PHEMA chains, respectively.

The linear decrease of the specific volume of the nanocomposites, with the silica content from 0.85 cm^3/g for H00 to 0.79 cm^3/g for H20, leads to a specific volume extrapolated for a sol–gel 100 wt % SiO_2 of 0.53 cm^3/g, which is lower than the values obtained by Brinker et al.[12] for acid-catalyzed silica gels using higher water/TEOS ratios (0.61–0.76 cm^3/g for water/TEOS ratios ranging from 4.2 to 15.3) and higher than the value of 0.45 cm^3/g of the pure silica glass obtained by those same authors by curing at 900°C. In Figure 7, the specific volumes calculated considering the most efficient packing of the phases with no interstitial vacancies, that is, all the silica pores occupied by the organic polymer chains, have also been represented as a straight line. For this purpose were used the specific volumes of PEMA, PHEA (measured by us), and that of pure SiO_2 glass (taken from Ref. 12), and their corresponding mass fractions. The difference points to the nanoporosity of the structure of silica obtained by this procedure.

Regarding the porosity of the scaffolds, looking at the micrographies, neither the pore diameter nor their distribution seem to vary significantly with the composition. The porosity of the PHEA scaffold is lower than that of the PEMA scaffold (Table II), probably because of the shrinkage of the PHEA scaffold, which is a rubber at room temperatures while PEMA is a glass in these conditions. The porosity of the copolymer is lower than that of the PEMA scaffold; the presence of PHEA probably provoked a small shrinkage. The porosity of the hybrids is scarcely affected by the different silica contents and takes similar values to that of the PEMA scaffold, suggesting that the shrinkage of the matrix is prevented by the presence of silica.

The EWC of the P(EMA-*co*-HEA) copolymer resembles more that of PEMA than that of PHEA: a linear combination of the specific swelling capacities of both pure homopolymers would give an EWC of 60.76% for the copolymer, instead of the experimental 8.34% (Table I). The discrepancy of the true EWC from this simple linear prediction can be explained by the fact that the copolymer network is much more rigid (has a higher T_g and is a glass at room temperature) than the rubbery PHEA network, and thus cannot expand as much as does the PHEA while it absorbs water, giving rise to this strongly nonlinear swelling. Additionally, this higher rigidity of the copolymer main chains could also render more stable micellized associations of the —OH groups of the HEA side chains, leaving them inaccessible as sorption sites.

In the case of the hybrid materials the water sorption capacity referred to the HEA mass in the sample (EWC′) is almost constant for the different silica contents, and equal to that of the copolymer (Table I). This must be interpreted as a strong indication that the water sorption ability of the hybrids is still due essentially to their HEA component, and that this unit is as hydrophilic in the nanocomposites as it is in the copolymer. The presence of silica does not seem to have influence on the water sorption of the copolymer. This means that condensation reactions between silica and the organic polymer, if existent at all, must involve a negligible number of HEA units.

Concerning the mechanical spectra, the copolymer shows the glass–rubber relaxation as a sharp single drop of

the storage modulus to very low values, with the corresponding maximum of the loss tangent, which is indicative of the homogeneity of the copolymer and the inexistence of different phase-separated domains. With the increase of silica content, the glass–rubber relaxation gradually broadens, decreases in intensity, and shifts to higher temperatures. The modulus in the rubbery region increases following an exponential tendency, as can be observed in the inset of Figure 9. The inorganic network produces a reinforcing effect by constraining the long distance cooperative motions of the copolymer main chains and immobilizing the polymer chains at the organic–inorganic interface, as was also found when the silica phase consists of beads.[50] The strong increase of the rubbery plateau modulus from the 10 wt % of silica content on must be related to the percolation of the silica phase, forming a continuously extended network throughout the sample for silica contents higher than that threshold.[11,43,51] The fact that only for these silica contents a continuous densified silica structure was obtained after pyrolysis at 1000°C during 4 h and removal of the organic phase is consistent with this observation. Other authors[30] attributed analogous DMS observations in the PHEMA/SiO_2 system to heterocondensation reactions of the polymer chains and the silica network, leading also to relatively stronger inter- and intramolecular hydrogen bonding. In our case, this explanation would be difficult to reconcile with the impoverished thermal stability of the hybrids.

At temperatures higher than 150°C, a slight aging phenomenon seems to occur, that is, the storage modulus increases additionally. Probably, this happens because molecular motions at these supra-T_g temperatures allow previously frozen sol–gel reactions to complete, leading to a slightly increased connectivity of the silica network. Such an effect has been previously reported.[11]

The elastic modulus of the copolymer scaffold is very close to that of PEMA (Table II). Silica contents above 5% lead to an increase in the compressive Young modulus over the PEMA value, up to 6238 MPa for H20. This is in agreement with the DMS observations. The elastic modulus of the hybrids increases with the HAp coating. The HAp-coated H15 scaffold has an elastic modulus of 8192 MPa. This elastic modulus is still lower than that of human dentin, which is 14.47 GPa.[53] It is expected that, when the scaffolds will be implanted *in vivo*, the regenerated tissue will contribute to the definitive compressive modulus.

The SBF *in vitro* test gives a good indication of the ability of materials to nucleate and grow apatite on their surfaces in the living body, and thus an indication of final bonding to the living bone.[23,15] In a previous work (unpublished observation) the ability of this series of hybrid materials to form HAp on their surfaces was studied *in vitro* by soaking bulk samples (8 mm diameter, 0.8 mm thickness) in SBF solution for different times up to 35 days. The composition and morphology of the HAp layer formed were characterized by SEM, EDS, FTIR, and XRD, and additionally the exchange of soluble silicates and calcium and phosphate ions at the interface, and the structural changes taking place in the nanohybrids when immersed in SBF were analyzed by SEM-EDS. On the basis of those results, an apatite nucleation mechanism for these nanohybrids was advanced and correlated with the differing nanostructures of the materials as a function of their silica content. The nanohybrids with silica contents in the range of 10–20 wt % proved to be the most suitable for the development of bioactive synthetic scaffolds for bone or dentin, since the dissolution of silica at the surface was facilitated by the presence of large numbers of noncondensed silanol terminal groups in the silica network because of the still quite disconnected topology of the silica phase; the release of soluble silicates renders an interface layer rich in silanol groups. In this reaction zone of a few micrometers, calcium and phosphate ions are adsorbed and interact with the polar groups of soluble and hydrated silica to form calcium phosphates. Once apatite nuclei are formed (7 days), the growth of the apatite layer and formation of successive layers occur very rapidly in all cases. The initially amorphous calcium phosphate, containing other ions such as CO_3^{2-}, Na^+, K^+, or Mg^{2+} stabilizes, leading to low-crystalline nanocrystallites of calcium-deficient carbonated-HAp, with Ca/P ratios near the physiological HAp ratio. Above a silica concentration threshold of ~20 wt %, the continuously extended dense silica interpenetrated network hinders the organic polymer network expansion and the diffusion of Ca^{2+} ions, and has a lower density of surface silanols, leading to a lesser hydrolysis of the silica network at the interface, and thus the nucleation of HAp occurs even more slowly than on the copolymer surface (where only the carboxyl and hydroxyl groups induce the HAp nucleation). At the end of the test (35 days), the surfaces of all the hybrids and the copolymer were similar.

In this work, we assessed the bioactivity of the single H15 scaffold, since the purpose now was not to confirm our previous findings on the bulk materials but to evaluate the effect of scaffold architecture on the apatite coating formation. Problems such as the influence of the strongly curved geometries of the substrate onto which the apatite layer grows and whether this layer would blind the tubule apertures needed to be investigated. In general, 7 days do not seem to be a sufficient time to induce the nucleation of apatite in the interior of the tubules of the H15 scaffolds. Nonetheless, the soaking in 2×SBF during 7 more days promotes the accelerated deposition of aggregates on the surface, including the inner surfaces of the pores. These aggregates present the typical cauliflower structures of HAp needle-shaped crystals observed previously on the bulk samples, with a composition similar to that of stoichiometric HAp. As a consequence the average tubule diameter decreases from 8 to ~5 μm. This new pore diameter resembles more that of the natural dentinal tubule (~2.5 μm near the pulp and 0.9 μm near the dentin–enamel junction[2]), being thus more convenient for the proposed

application. The apatite coating of the pores and the consequent decrease in tubule diameter and mechanical reinforcement are very interesting features in the way to mimic natural dentin with regard to its structure, morphology (porosity and tubule diameter), and mechanical properties.

CONCLUSIONS

A series of silica-based organic–inorganic nanocomposite scaffolds, with varying proportions of silica up to 20 wt %, were prepared and characterized, with the aim of mimicking the structure and properties of mineralized tissue from natural dentin. With this purpose, P(EMA-*co*-HEA) 70/30 wt % and silica were simultaneously polymerized by the sol–gel method, using a PAN fiber template that was eventually eliminated to leave homogeneously distributed aligned tubular pores of $\sim$8 μm of diameter.

The TEOS as silica precursor was efficiently hydrolyzed and condensed to silica during the sol–gel process, and silica was found to be present not only in the bulk, but also on the outer and inner (pore) surfaces of the hybrids, conferring them bioactivity when immersed in body fluids. Silica contents above 10 wt % resulted in continuous silica networks interpenetrated with the organic phase, which produced a reinforcing effect in the polymeric matrix, evidenced by the hindered long-range motions of copolymer main chains, altered shrinkage, and swelling.

The porous hybrid structures here obtained, capable of inducing the deposition of apatite on their surfaces *in vitro*, resemble natural dentin with regard to its structure and properties. The obtained results strongly suggest these nanohybrids as suitable substrates for the regeneration of dental mineralized tissue.

REFERENCES

1. Marshall GW, Marshall SJ, Kinney JH, Balooch M. The dentin substrate: Structure and properties related to bonding. J Dent 1997;25:441–458.
2. Spencer P, Wang Y, Katz JL. Dentin. In: Akay M, editor. Wiley Encyclopedia of Biomedical Engineering. New Jersey: Wiley; 2006. p 1051–1060.
3. Bohl KS, Shon J, Rutherford B, Mooney DJ. Role of synthetic extracellular matrix in development of engineered dental pulp. J Biomater Sci Polym Ed 1998;9:749–764.
4. Nakashima M. Bone morphogenetic proteins in dentin regeneration for potential use in endodontic therapy. Cytokine Growth Factor Rev 2005;16:369–376.
5. Young CS, Terada S, Vacanti JP, Honda M, Bartlett JD, Yelick PC. Tissue engineering of complex tooth structures on biodegradable polymer scaffods. J Dent Res 2002;81:695–700.
6. Yelick PC, Vacanti JP. Bioengineered teeth from tooth bud cells. Dent Clin North Am 2006;50:191–203.
7. Buurma B, Gu K, Rutherford RB. Transplantation of human pulpal and gingival fibroblasts attached to synthetic scaffolds. Eur J Oral Sci 1999;107:282–289.
8. Dobie K, Smith G, Sloan AJ, Smith AJ. Effect of alginate hydrogels and TGF-β1 on human dental pulp repair in vitro. Connect Tissue Res 2002;43:387–390.
9. Vidaurre A, Cortazar IC, Meseguer JM. Water sorption properties of poly(ethyl acrylate-*co*-hydroxyethyl methacrylate) macroporous hydrogels. Macromol Symp 2003;200:283–290.
10. Stokols S, Sakamoto J, Breckon C, Holt T, Weiss J, Tuszynski MH. Templated agarose scaffolds support linear axonal regeneration. Tissue Eng 2006;12:2777–2787.
11. Hajji P, David L, Gerard JF, Pascault JP, Vigier G. Synthesis, structure, and morphology of polymer-silica hybrid nanocomposites based on hydroxyethyl methacrylate. J Polym Sci Part B: Polym Phys 1999;37:3172–3187.
12. Brinker CJ, Keefer KD, Schaefer DW, Ashley CS. Sol–gel transition in simple silicates. J Non-Cryst Solids 1982;48:47–64.
13. Jackson CL, Bauer BJ, Nakatani AI, Barnes JD. Synthesis of hybrid organic–inorganic materials from interpenetrating polymer network chemistry. Chem Mater 1996;8:727–733.
14. Hench LL. The story of bioglass. J Mater Sci Mater Med 2006;17:967–978.
15. Kokubo T. Bioactive glass ceramics: Properties and applications. Biomaterials 1991;12:155–163.
16. Ohtsuki C, Kokubo T, Yamamuro T. Mechanism of apatite formation on CaO-SiO_2-P_2O_5 glasses in a simulated body fluid. J Non-Cryst Solids 1992;143:84–92.
17. Li R, Clark AE, Hench LL. An investigation of bioactive glass powders by sol–gel processing. J Appl Biomater 1992;2:231–239.
18. Salinas AJ, Vallet-Regí M, Izquierdo-Barba I. Biomimetic apatite deposition on calcium silicate gel glasses. J Sol-Gel Sci Tech 2001;21:13–25.
19. Takadama H, Kim HM, Kokubo T, Nakamura T. Mechanism of biomineralization of apatite on a sodium silicate glass: TEM-EDX study *in vitro*. Chem Mater 2001;13:1108–1113.
20. Kim HM, Himeno T, Kawashita M, Kokubo T, Nakamura T. The mechanism of biomineralization of bone-like apatite on synthetic hydroxyapatite: An *in vitro* assessment. J R Soc Interface 2004;1:17–22.
21. Kim HM, Himeno T, Kokubo T, Nakamura T. Process and kinetics of bonelike apatite formation on sintered hydroxyapatite in a simulated body fluid. Biomaterials 2005;26:4366–4373.
22. Vallet-Regí M, Salinas AJ, Arcos D. From the bioactive glasses to the star gels. J Mater Sci Mater Med 2006;17:1011–1017.
23. Kokubo T, Takadama H. How useful is SBF predicting in vivo bone bioactivity? Biomaterials 2006;27:2907–2915.
24. Ohtsuki C, Kamitakahara M, Miyazaki T. Coating bone-like apatite onto organic substrates using solutions mimicking body fluid. J Tissue Eng Regen Med 2007;1:33–38.
25. Eglin D, Maalheem S, Livage J, Coradin T. In vitro apatite forming ability of type I collagen hydrogels containing bioactive glass and silica sol–gel particles. J Mater Sci Mater Med 2006;17:161–167.
26. Oréfice R, Clark A, West J, Brennan A, Hench L. Processing, properties, and *in vitro* bioactivity of polysulfone-bioactive glass composites. J Biomed Mater Res A 2007;80:565–580.
27. Yu S, Hariram KP, Kumar R, Cheang P, Aik KK. In vitro apatite formation and its growth kinetics on hydroxyapatite/polyetheretherketone biocomposites. Biomaterials 2005;26:2343–2352.
28. Fang L, Leng Y, Gao P. Processing of hydroxyapatite reinforced ultrahigh molecular weight polyethylene for biomedical applications. Biomaterials 2005;26:3471–3478.
29. Li Z, Yubao L, Aiping Y, Xuelin P, Xuejiang W, Xiang Z. Preparation and *in vitro* investigation of chitosan/nano-hydroxyapatite composite used as bone substitute materials. J Mater Sci Mater Med 2005;16:213–219.

30. Huang SL, Chin WK, Yang WP. Structural characteristics and properties of silica/poly(2-hydroxyethyl methacrylate) (PHEMA) nanocomposites prepared by mixing colloidal silica or tetraethyloxysilane (TEOS) with PHEMA. Polymer 2005;46:1865–1877.
31. Constantini A, Luciani G, Annunziata G, Silvestri B, Branda F. Swelling properties and bioactivity of silica gel/pHEMA nanocomposites. J Mater Sci Mater Med 2006;17:319–325.
32. Liu YL, Hsu CY, Hsu KY. Poly(methylmethacrylate)-silica nanocomposites films from surface-functionalized silica nanoparticles. Polymer 2005;46:1851–1856.
33. Tsuru K, Ohtsuki C, Osaka A, Iwamoto T, Mackenzie JD. Bioactivity of sol-gel derived organically modified silicates. I. In vitro examination. J Mater Sci Mater Med 1997;8:157–161.
34. Ohtsuki C, Miyazaki T, Tanihara M. Development of bioactive organic–inorganic hybrid for bone substitutes. Mater Sci Eng C 2002;22:27–34.
35. Ohtsuki C, Miyazaki T, Kamitakahara M, Tanihara M. Design of novel bioactive materials through organic modification of calcium silicate. J Eur Ceram Soc 2007;27:1527–1533.
36. Abe Y, Kokubo T, Yamamuro T. Apatite coating on ceramics, metals and polymers utilizing a biological process. J Mater Sci Mater Med 1990;1:233–238.
37. Tanahashi M, Yao T, Kokubo T, Minoda M, Miyamoto T, Nakamura T, Yamamuro T. Apatite coating on organic polymers by a biomimetic process. J Am Ceram Soc 1994;77: 2805–2808.
38. Kim HM, Kishimoto K, Miyaji F, Kokubo T, Yao T, Suetsugu Y, Tanaka J, Nakamura T. Composition and structure of the apatite formed on PET substrates in SBF modified with various ionic activity products. J Biomed Mater Res 1999;46:228–235.
39. Oliveira AL, Malafaya PB, Reis RL. Sodium silicate gel as a precursor for the in vitro nucleation and growth of a bone-like apatite coating in compact and porous polymeric structures. Biomaterials 2003;24:2575–2584.
40. Bosch P, Del Monte F, Mateo JL, Levy D. Photopolymerization of hydroxyethylmethacrylate in the formation of organic–inorganic hybrid sol–gel matrices. J Polym Sci Part A: Polym Chem 1996;34:3289–3296.
41. Rhee SH, C JY, Kim HM. Preparation of a bioactive and degradable poly(ε-caprolactone)/silica hybrid through a sol–gel method. Biomaterials 2002;23:4915–4921.
42. Costa ROR, Vasconcelos WL. Structural modification of poly(2-hydroxyethyl methacrylate)-silica hybrids utilizing 3-methacryloxypropyltrimethoxysilane. J Non-Cryst Solids 2002; 304:84–91.
43. Lin DJ, Chen CC, Su YC, Huang SH, Cheng LP. Preparation of silica-filled poly(2-hydroxymethylmethacrylate) nanocomposites cured by photoirradiation during the sol–gel process. J Appl Polym Sci 2004;94:1927–1935.
44. Pereira MM, Jones JR, Orefice RL, Hench LL. Preparation of bioactive glass–polyvinyl alcohol hybrid foams by the sol–gel method. J Mater Sci Mater Med 2005;16:1045–1050.
45. Yoldas BE. Introduction and effect of structural variations in inorganic polymers and glass networks. J Non-Cryst Solids 1982;51:105–121.
46. Rhee SH. Effect of molecular weight of poly(ε-caprolactone) on interpenetrating network structure, apatite-forming ability, and degradability of poly(ε-caprolactone)/silica nano-hybrid materials. Biomaterials 2003;24:1721–1727.
47. Costa ROR, Lameiras FS, Vasconcelos WL. Structural control in poly(butyl acrylate)-silica hybrids by modifying polymer–silica interactions). J Sol-Gel Sci Tech 2003;27:343–354.
48. Costa ROR, Pereira MM, Lameiras FS, Vasconcelos WL. Apatite formation on poly(2-hydroxyethyl methacrylate)-silica hybrids prepared by sol–gel process. J Mater Sci Mater Med 2005;16:927–932.
49. Strawbridge I, Craievich AF, James PF. The effect of the H_2O/TEOS ratio on the structure of gels derived by the acid catalysed hydrolysis of tetraethoxysilane. J Non-Cryst Solids 1985;72:139–157.
50. Goertzen WK, Kessler MR. Dynamic mechanical analysis of fumed silica/cyanate ester nanocomposites. Compos A 2008; 39:761–768.
51. Bandyopadhyay A, Bhowmick AK, De Sarkar M. Shyntesis and characterization of acrylic rubber/silica hybrid composites prepared by sol–gel technique. J Appl Polym Sci 2004;93:2579–2589.
52. Craig RG, Peyton FA. Elastic and mechanical properties of human dentin. J Dent Res 1958;37:710–718.